




The effect of cooling rate on the microstructure and mechanical properties of NiCoFeCrGa high-entropy alloy

Dávid Molnár^{1,2}, Ádám Vida^{3,4}, Shuo Huang¹, and Nguyen Q. Chinh^{4,*} 

¹Applied Materials Physics, Department of Materials Science and Engineering, Royal Institute of Technology, 100 44 Stockholm, Sweden

²Materials Science Group, Dalarna University, 791 88 Falun, Sweden

³Institute for Solid State Physics and Optics, Wigner Research Centre for Physics, P.O. Box 49, Budapest 1525, Hungary

⁴Department of Materials Physics, Eötvös University Budapest, Pázmány P. sétány 1/A, Budapest 1117, Hungary

Received: 13 August 2018

Accepted: 26 November 2018

© Springer Science+Business Media, LLC, part of Springer Nature 2018

ABSTRACT

The effect of cooling rate on the microstructure and mechanical properties of equimolar NiCoFeCrGa high-entropy alloy (HEA) was studied by scanning electron microscopy, energy-dispersive X-ray spectroscopy and electron backscatter diffraction (EBSD), as well as by microhardness tests. Experimental results show that the cooling rate has a crucial impact on the developing microstructure which has a mixture of two—FCC and BCC—phases, leading to a self-similarity of the solidified structure formed in the sample. Furthermore, the cooling rate influences both the composition of the two phase-components and the ratio of their volume fractions, determining the mechanical properties of the sample. The present results confirm the grouping of Co, Fe and Cr in the FCC phase and that of Ni and Ga in BCC phase in the NiCoFeCrGa high-entropy alloy system. An empirical rule is suggested to predict how the phase-components can be expected in this complex high-entropy alloy.

Introduction

High-entropy alloys (HEAs) are novel multicomponent alloys containing at least 4–5 components in equimolar or near-equimolar composition [1–5]. This new type of alloy opened up a new area in materials science due to its excellent mechanical [6, 7], magnetic [8–10] and oxidation [11] properties. The HEAs can solidify either in single-phase solid solutions or

in multiphase structures having a mixture of simple phases such as body-centered cubic (BCC), face-centered cubic (FCC) or hexagonal close-packed (HCP) [12–14]. So far, it is established that the microstructure of a HEA is dominantly determined by the valence electron concentration (VEC) of the given composition [15]. For VEC values between 6.87 and 8, a mixture of FCC and BCC phases is expected [15, 16]. Below and above this interval, the formation

Address correspondence to E-mail: chinh@metal.elte.hu

of BCC and FCC single phases, respectively, takes place. In the region of mixture, one can fine-tune the system by composition in order to balance, for instance, the ratios of FCC and BCC phases in the duplex alloy to get a reasonable ductile–brittle trade-off for the mechanical and plastic properties of the materials [17, 18]. The good tunability of the HEAs can also be expanded to their magnetic properties. Recently, enhanced attentions were paid to the composition-tunable metastability of high-entropy alloys [18].

Despite many well-known features of the metastability of HEAs, some challenging tasks still remain, such as the effect of different heat treatments, the question of phase stabilities, the problem of large-scale castings [19] or the confirmation of the indicating role of the VEC number. Furthermore, similarly to bulk metallic glasses [20], the cooling rate might have a critical role in the developing microstructure and therefore in the properties of the high-entropy alloys [21, 22]. A minor difference in the cooling rate may lead to a significant change in the chemical distribution and, thus, in the microstructure. In the case of common castings, where the piece of sample can cool down in atmospheric conditions and not inside of a furnace, one will obtain a material which is far from the stable state. Further homogenization after casting must be applied in order to reach ordered (stable) microstructure. Since HEAs have a lot of degrees of freedom when it comes to preparation, simple guidelines are needed to predict the properties of the finished sample [23–25]. These predictions are either based on some simple parameters such as valence electron concentration (VEC) [15, 16], enthalpy of mixing, melting point, etc., or based on computationally more demanding methods such as *ab initio* calculations or CALPHAD [10, 26, 27].

The present study is a continuation of started works [28–30] dealing with the microstructures and mechanical properties of the NiCoFeCrGa high-entropy alloys, which can be considered as a good candidate for magnetocaloric applications [31]. The addition of Ga to the NiCoFeCr system turns the

originally paramagnetic alloy into a macroscopically ferromagnetic alloy by a new ferromagnetic BCC phase [28–30]. The aim of this work is to study widely the effect of cooling rate on the microstructure and mechanical properties of an equal-molar Ni₂₀Co₂₀Fe₂₀Cr₂₀Ga₂₀ high-entropy alloy.

Experimental procedures

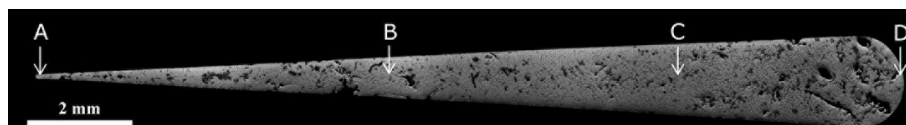
High-purity elements (99.99% delivered by Johnson Matthey company) were used to prepare the Ni₂₀Co₂₀Fe₂₀Cr₂₀Ga₂₀ sample having a total mass of 20 g (composition in at%). The ingot was melted at about 1800 °C in a water-cooled copper mold using induction melting. Ar gas with titanium getter was used to prevent the sample from oxidation. The melting process was repeated five times to achieve homogeneity of the sample. As the master alloy was ready, it was placed and remelted in a centrifugal casting equipment and spin-cast into a wedge-shaped copper mold. This type of mold allows us to investigate the effect of different cooling rates in a single specimen due to the varying thickness along the sample. We note here that in some earlier studies dealing with cooling rate effects of NiCoFeCr-based HEA alloys [21, 22] the different cooling rates were achieved by changing the casting method.

Figure 1 shows the optical image of the investigated NiCoFeCrGa HEA sample. According to the empirical relation suggested by Pryds and Huang [32], the cooling rate of different (*d*) thickness parts of the wedge is reciprocally proportional to *d*² so that the cooling rate ($\sim 10^5$ K/s at the tip (point A) is about three orders of magnitude higher than that ($\sim 10^2$ K/s at the bottom (point D).

The surface of the sample was prepared by grinding and consecutively finer steps of polishing, where Struers OP-S colloidal silica was used as the final step of the polishing.

To analyze the microstructure and the phases, a Zeiss Ultra 55 FEG-SEM was used with an Oxford PentaFETx3 EDS and an Oxford Instruments HKL Nordlys F EBSD system. The acceleration voltage was set to 15 kV with high-current mode; the working

Figure 1 Optical image of the *xy* surface of the spin-cast sample.



distance was 20.2 mm for EBSD and 8.5 mm for EDS; and the aperture was set to 120 μm .

Microindentation tests were carried out by a CSM Micro Combi Tester (MCT) using a diamond Vickers indenter. The maximum load of 100 g was applied at the loading rate of 3.3 g/s. Indentations were carried out along the centerline (as the x -direction) at every 200 μm . At each position, two indents were done for a distance of 50 μm in the y -direction and the average hardness of them was used as the value describing the given x -position. Oliver–Pharr method [33] was used for evaluating the indentation measurements.

Results and discussion

It was shown previously that the base NiCoFeCr alloy contains only a single FCC phase microstructure with VEC value of 8.25 [16, 28]. With Ga addition, the average VEC value drops down to 7.2 and in agreement with the VEC rule described before. The NiCoFeCrGa contains both BCC and FCC phases, which was confirmed by XRD and also by EBSD measurements [28]. In the present work, the ratio of these two phases and their effect on the mechanical properties are discussed. All the measurements—EBSD, EDS and microhardness—were taken along the centerline of the sample (shown in Fig. 1) between the tip (on the left in x -direction) and the

bottom (on the right) of the sample. The scale starts from the tip (0 mm) and ends at the bottom (17 mm) along the centerline going through the middle of the sample.

The SEM images of Fig. 2 show the microstructures of the different (marked by A, B, C and D) positions of the investigated alloy. The images were taken by using the backscattered electrons, making the contrast by the different atomic compositions of the phases. In all positions (from $x \approx 0$ to $x \approx 17$ mm) multiphase—dendritic—structure containing darker (dendrite) and brighter (inter-dendrite) regions can be observed. This multiphase structure is in agreement with the mentioned VEC criteria predicted by Sheng Guo et al. [15]. It can be seen that the size of the local dendrite/inter-dendrite regions strongly depends on the investigated position due to the different cooling rates along the wedge, but the phase structure remains the same. In the previous studies [21, 22] on the microstructures of other NiCoFeCr-based alloys, it was shown that the cooling rate may affect not only the phase fractions and morphologies, but also the type of the microstructure.

The results of the EBSD investigations show that the dendrite areas in the images mark the FCC phase and the inter-dendrite ones present the BCC phase regions. The compositions of the different phases shown in the SEM images were analyzed by EDS measurements and are given in Table 1. It can be seen

Figure 2 Backscattered electron images of the areas in positions A, B, C and D measured by EDS. The corresponding data are summarized in Table 1. The inset A* shows a magnified area from the position A, and inset D* shows an area with lower magnification from the position D.

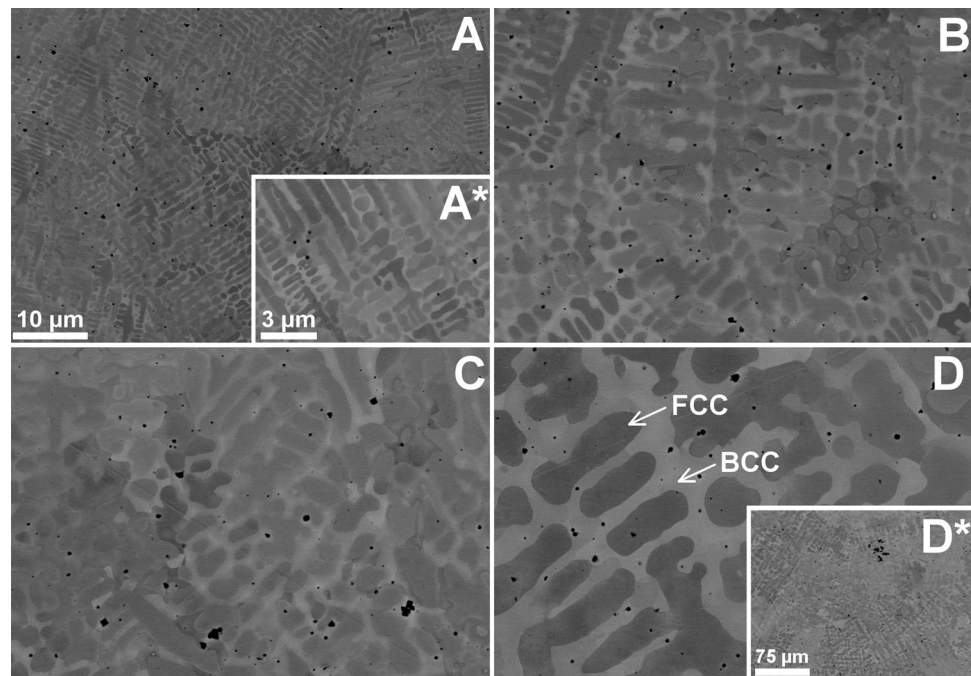


Table 1 Concentrations of the elements along the sample, measured by EDS

SEM area	Distance from tip (mm)	Dendrite (FCC)/inter-dendrite (BCC)	Concentration (at%)					Cooling rate (K/s)	VEC
			Cr	Fe	Co	Ni	Ga		
A.	0	I	19.33	19.21	19.77	20.13	21.56	$\sim 10^5$	7.14
		D	19.38	19.98	20.4	19.68	20.57		7.18
B.	7	I	18.25	17.55	18.62	21.43	24.15	$\sim 10^3$	7.04
		D	20.58	21.64	21.42	18.32	18.04		7.27
C.	13	I	17.97	17.32	18.27	21.7	24.75	$\sim 10^3$	7.02
		D	20.28	21.25	21.13	18.68	18.67		7.25
D.	17	I	15.96	16.82	17.78	21.86	27.58	$\sim 10^2$	6.92
		D	22.76	22.65	22.3	17.87	14.41		7.40

that at all positions, the FCC phase—the dendrites—is more rich in Fe, Co and Cr and the BCC phase—the inter-dendrite—contains more Ni and Ga. This result is well established in our previous work [29]. Based on the grouping of Co, Fe and Cr, as well as of Ni and Ga, it was supposed that during the solidification, the first step of the crystallization is the formation of the FCC phase containing higher amount of Fe and Cr, which elements have the highest melting points. Then, the melting point of the remaining melt decreases, leading to the formation of the BCC phase from rather the lower-melting-point components.

It can be also observed that the composition of both FCC (dendrite) and BCC (inter-dendrite) regions changes along the sample due to the change in the cooling rate. In Fig. 3, we present the concentration of the elements in the dendritic and inter-dendritic regions for low cooling rate (bottom of the sample) and high cooling rate (tip of the sample). It is well visible that the elements are separated into two groups. In the inter-dendritic region (BCC phase), the concentration of Ni and Ga is higher at the tip of the sample compared to the other three elements, Fe, Cr and Co, respectively. These observations suggest that the cooling rate is important not only when it comes to the development of the different crystal structures, but it has a crucial impact on the composition of those phases as well. In the rapid cooling parts, the nominal 20 at% concentration for all elements can be observed within the error. This is a natural consequence of quick cooling on diffusion-controlled processes. In general, the diffusion in HEAs can be more complicated for elements due to the severely distorted lattice [22, 34]. It is also worth mentioning that the cooling rate affects the size of the dendrites. The spacing of the dendrite arms is larger for lower

cooling rates ($\sim 10^2$ K/s) and smaller for higher cooling rates ($\sim 10^5$ K/s) which means that for a given length, more and thinner dendrite arms will develop at high cooling rates, as well as less and thicker dendrite arms form at lower cooling rates. This trend is clearly visible in Fig. 2, where small and dense ($\sim 1\text{-}\mu\text{m}$ spacing) dendrites can be observed in the **A** inset, while large and sparse ($\sim 5\text{-}\mu\text{m}$ spacing) dendrites can be seen in the **D** inset.

Considering again the cooling rates of different parts of the specimen, it should be noted that in spite of different sizes of local dendrite/inter-dendrite regions, the microstructures obtained at different cooling rates seem to be self-similar. The insets **A*** and **D*** in Fig. 2 show a higher and lower magnified areas of the positions **A** and **D**, respectively. It can be seen that when applying proper (different) magnifications, the microstructures observable at different positions (e.g., at positions **A** and **D**)—for different cooling rates—could not be distinguished. Our experimental results show that a very fine distribution of the dendrite/inter-dendrite self-similar structures should form very quickly at the beginning of the casting process and then different parts of it grow by the diffusion of the composing atoms as facilitated by the decrease in the cooling rate at an increasing thickness of the cast sample. The subsequent diffusion of the composing atoms also leads to the change in the composition of the two (FCC and BCC) phases, as shown in Table 1 and Fig. 3. Considering both the very high cooling rate ($\sim 10^5$ K/s) at the tip of the sample and the mentioned self-similarity of the solidified structure, the results suggest that the separation of the phases may start in the liquid state above the liquidus temperature of the sample. Further investigation is needed to clarify this

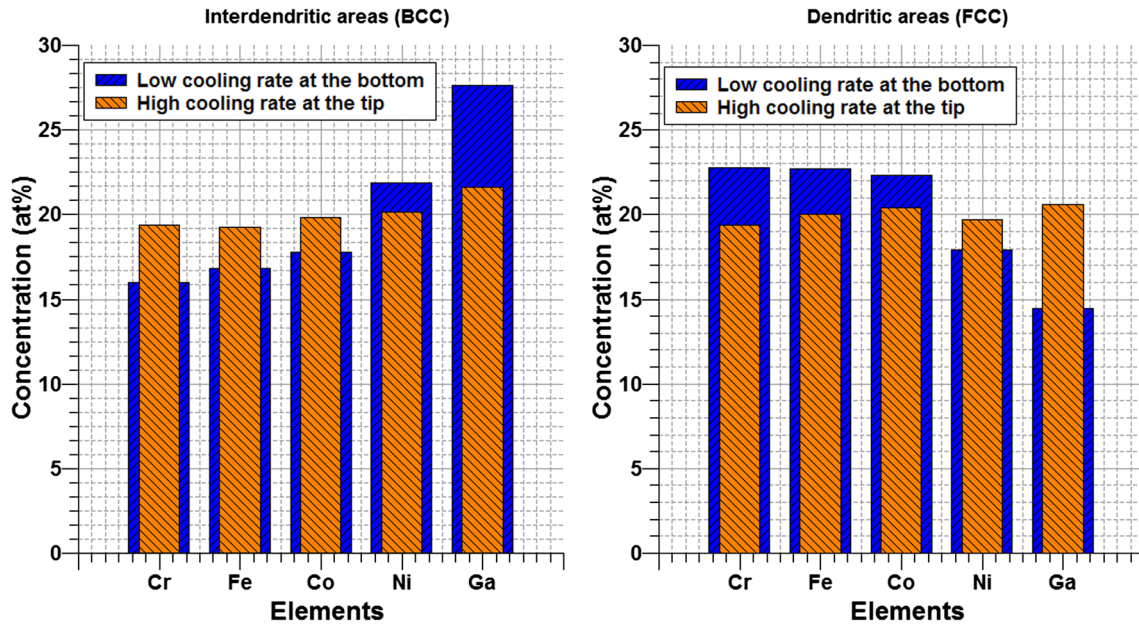


Figure 3 Concentration of the elements in the inter-dendritic (left panel) and dendritic (right panel) areas at the tip and the bottom of the sample.

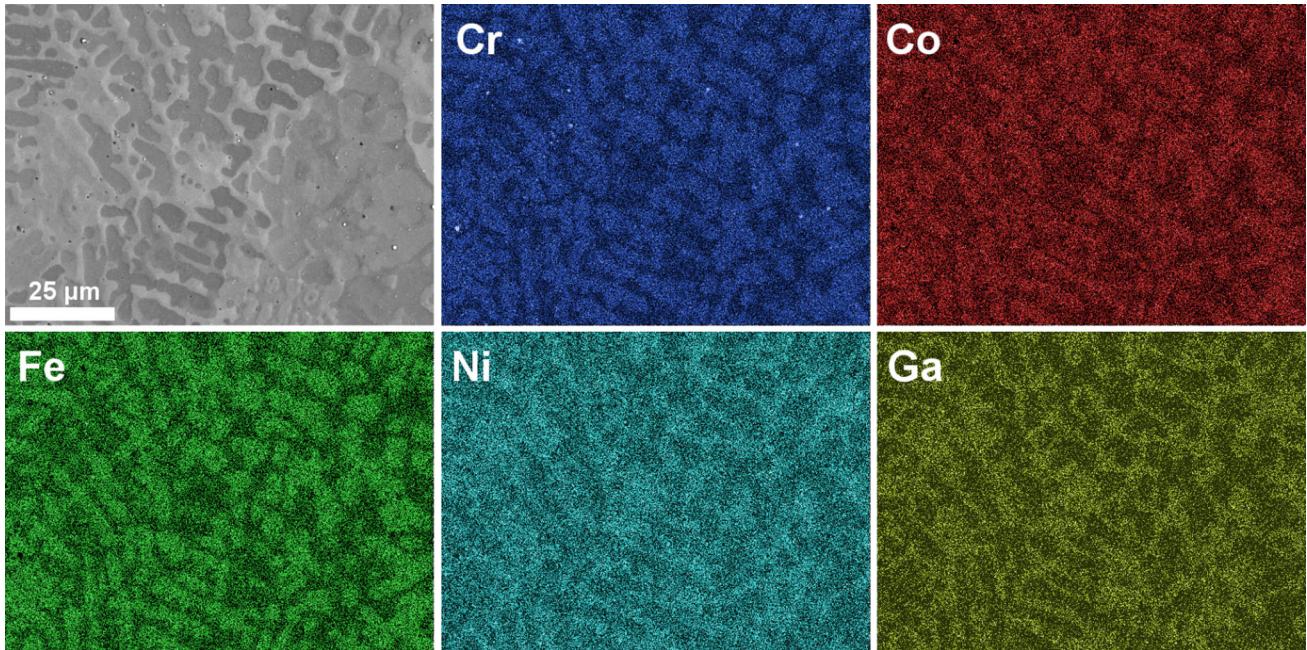


Figure 4 SEM and EDS images of the alloy around site D, showing visibly the grouping of Cr, Co and Fe and that of Ni and Ga atoms.

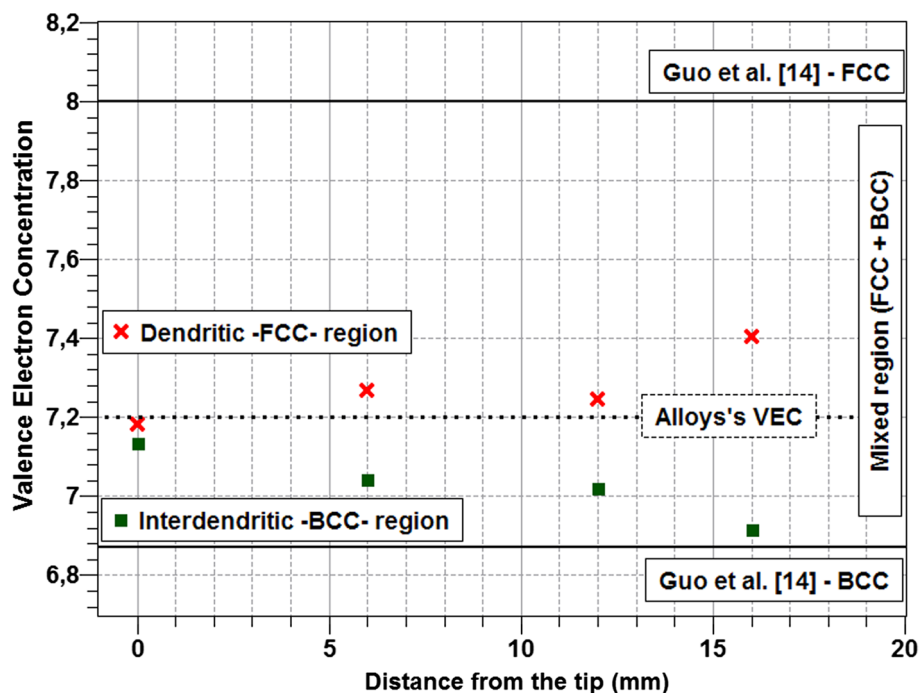
question in the present high-entropy NiCoFeCrGa alloy, where the mixing of the composing atoms may be more complicated than in conventional alloys.

Figure 4 shows the elemental maps taken in the vicinity of site D. The maps built from EDS measurements reveal clearly the same contours in Cr, Co

and Fe, as well as the similar profiles of Ni and Ga elements, confirming the grouping of Cr, Co and Fe and that of Ni and Ga atoms in the NiCoFeCrGa HEA system.

The grouping of Co, Fe and Cr, as well as of Ni and Ga seems to be well established. According to A.

Figure 5 VEC of the decomposed components calculated from the concentrations acquired by EDS measurements. Solid line shows the limits defined by Guo et al. The dotted line is the nominal VEC of the alloy.



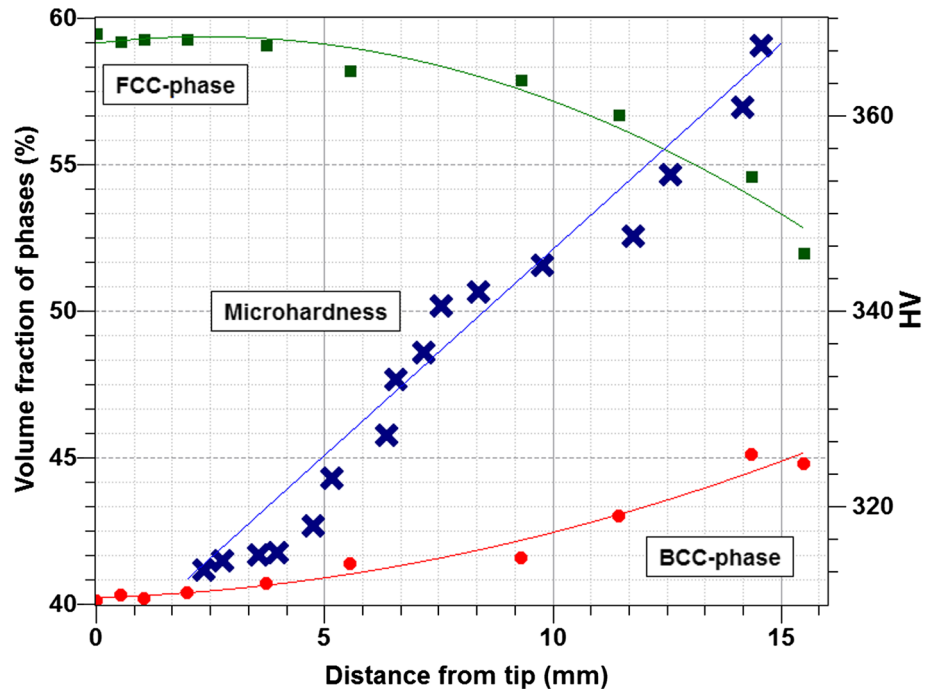
Takeuchi and A. Inoue [35], the mixing enthalpy (ΔH) of these components is the most negative between Ni and Ga. This thermodynamic reason explains why they can be found together. This factor certainly contributes to the formation of the FCC phase containing higher amount of Fe, Cr and Co and subsequently to the formation of the BCC phase with higher amount of Ni and Ga.

As it was mentioned, in general, the parameter VEC can be used in the design of HEAs to predict the crystal structure of the alloy [15, 16]. Considering the composition of FCC and BCC phases in the present work, the average VEC of 7.2 calculated for the equal-molar $\text{Ni}_{20}\text{Co}_{20}\text{Fe}_{20}\text{Cr}_{20}\text{Ga}_{20}$ sample is changing in different phases with different compositions. Figure 5 shows the VEC number of the phases formed at the positions A, B, C and D (see Fig. 1) along the centerline of the wedge-shaped sample. Our experimental results suggest an empirical rule to see how the (FCC and BCC) subphases can be expected in the NiCoFeCrGa system. Namely, the average VEC value of 7.2 seems to be a reasonable dividing line in between the FCC and BCC phases of the decomposed components. In the region of mixture (for VEC number between 6.87 and 8), the substructure will be BCC for VEC value below 7.2 and FCC for VEC value above 7.2.

In order to estimate the collective effect of the phases on the mechanical properties of the sample, microhardness measurements were taken along the centerline, and the results are shown in Fig. 6, where the volume fractions of the phases are also represented. Together with the variation of the composition described above, the volume fractions of the FCC and BCC phases are also monotonously decreasing from 60 to 55% and increasing from 40 to 45%, respectively, resulting in the increase of about 15% in the ratio of BCC/FCC from the tip to the bottom of the sample.

Applying the maximum load of 100 grams, the size of the Vickers patterns is about between 25 and 30 microns, covering several dendrites and inter-dendrites together. The results of hardness tests show clearly that the hardness (HV) is increasing from the tip to the bottom of the wedge, resulting in an increment of about 25% in hardness. Although the size of the components may also have an effect on the global strength, it should be emphasized that hardness change follows the trend of the ratio of BCC and FCC phases. The mixture of the soft and ductile FCC phase and the hard and brittle BCC component leads to a composite-like microstructure, the hardness of which is determined mainly by the volume fraction of the components. The 15% increase in the volume fraction of the BCC phase along the sample results

Figure 6 Microhardness values and volume fractions of phases as a function of the distance from the tip of the sample.



may certainly cause a 25% increment in hardness. The obtained experimental results confirm the strengthening effect of BCC phase in this type of HEA [28–30].

Conclusions

The effect of cooling rate on microstructure and mechanical properties of equimolar $\text{Ni}_{20}\text{Co}_{20}\text{Fe}_{20}\text{Cr}_{20}\text{Ga}_{20}$ high-entropy alloy was studied. Investigations were made on a wedge-shaped sample, which was prepared by centrifugal casting so that its different regions were cooled by different rates. The main results can be summarized as follows:

1. A mixture microstructure having FCC-phase dendrite and BCC-phase inter-dendrite is formed very quickly during the solidification of the sample. The size of the local dendrite/inter-dendrite regions strongly depends on the cooling rate, showing a self-similarity of the solidified structure and suggesting that the separation of the phases may start in the liquid state.
2. Experimental results show that the cooling rate influences both the composition of the two phase-components and the ratio of their volume fractions. Furthermore, independently of the cooling rate, the grouping of Co, Fe and Cr in FCC phase

and that of Ni and Ga in BCC phase is well established in the NiCoFeCrGa HEA system.

3. There is an unambiguous correlation between the hardness and the ratio of BCC/FCC phases. The obtained experimental results confirm the strengthening effect of BCC phase in this kind of mixture structure of HEAs.
4. Our results suggest an empirical rule to see how the (FCC and BCC) subphases can be expected in the NiCoFeCrGa system. In the region of mixture (for VEC number between 6.87 and 8), the substructure will be BCC for VEC value below 7.2 and FCC for VEC value above 7.2.

Acknowledgements

Dalarna University, Regional Development Council of Dalarna, Regional Development Council of Gävleborg, County Administrative Board of Gävleborg, Swedish Steel Producers' Association, Outokumpu Stainless and Sandviken City are thanked for financially supporting the research of DM. This research was partially supported by the Swedish Foundation for Strategic Research (SH), by the Hungarian–Russian Bilateral Research Program (TÉT) No. 2017-2.3.4-TÉT-RU-2017-00005, as well as by the Ministry of Human Capacities of Hungary within the

Eötvös University Excellence Program (1783-3/2018/FEKUTSRAT).

Data availability statement

The data that support the findings of this study are all own results of the authors and not available anywhere.

Compliance with ethical standards

Conflict of interest The authors declare that they have no conflict of interest.

References

- [1] Yeh JW, Chen SK, Lin SJ, Gan JY, Chin TS, Shun TT, Tsau CH, Chang SY (2004) Nanostructured high-entropy alloys with multiple principal elements: novel alloy design concepts and outcomes. *Adv Eng Mater* 6:299–303
- [2] Cantor B, Chang ITH, Knight P, Vincent AJB (2004) Microstructural development in equiatomic multicomponent alloys. *Mater Sci Eng A* 375:213–218
- [3] Miracle DB, Senkov ON (2017) A critical review of high entropy alloys and related concepts. *Acta Mater* 122:448–511
- [4] Ye YF, Wang Q, Lu J, Liu CT, Yang Y (2016) High-entropy alloy: challenges and prospects. *Mater Today* 19(6):349–362
- [5] Murty BS, Yeh JJW, Ranganathan S (2014) High-entropy alloys. Butterworth-Heinemann, Oxford
- [6] Deng Y, Tasan CC, Pradeep KG, Springer H, Kostka A, Raabe D (2015) Design of a twinning-induced plasticity high entropy alloy. *Acta Mater* 94:124–133
- [7] Laplanche G, Kostka A, Horst OM, Eggeler G, George EP (2016) Microstructure evolution and critical stress for twinning in the CrMnFeCoNi high-entropy alloy. *Acta Mater* 118:152–163
- [8] Huang S, Vida Á, Molnár D, Kádás K, Varga LK, Holmström E, Vitos L (2015) Phase stability and magnetic behavior of FeCrCoNiGe high-entropy alloy. *Appl Phys Lett* 107(25):251906
- [9] Koželj P, Vrtnik S, Jelen A, Jazbec S, Jagličić Z, Maiti S, Feuerbacher M, Steurer W, Dolinšek J (2014) Discovery of a superconducting high-entropy alloy. *Phys Rev Lett* 113(10):107001
- [10] Zhang Y, Zuo T, Cheng Y, Liaw PK (2013) High-entropy alloys with high saturation magnetization, electrical resistivity, and malleability. *Sci Rep* 3:1455
- [11] Fazakas É, Wang JQ, Zadorozhnyy V, Louzguine-Luzgin DV, Varga LK (2014) Microstructural evolution and corrosion behavior of Al₂₅Ti₂₅Ga₂₅Be₂₅ equi-molar composition alloy. *Mater Corros* 65:691–695
- [12] Zou Y, Ma H, Spolenak R (2015) Ultrastrong ductile and stable high-entropy alloys at small scales. *Nat Commun* 6:7748
- [13] Tracy CL, Park S, Rittman DR, Zinkle SJ, Bei H, Lang M, Ewing RC, Mao WL (2017) High pressure synthesis of a hexagonal close-packed phase of the high-entropy alloy CrMnFeCoNi. *Nat Commun* 8:15634
- [14] Wang WR, Wang WL, Wang SC, Tsai YC, Lai CH, Yeh JW (2012) Effects of Al addition on the microstructure and mechanical property of Al_xCoCrFeNi high-entropy alloys. *Intermetallics* 26:44–51
- [15] Guo S, Ng C, Lu J, Liu CT (2011) Effect of valence electron concentration on stability of fcc or bcc phase in high entropy alloys. *J Appl Phys* 109(10):103505
- [16] Tian F, Varga LK, Chen N, Shen J, Vitos L (2015) Empirical design of single phase high-entropy alloys with high hardness. *Intermetallics* 58:1–6
- [17] Lu Y, Dong Y, Guo S, Jiang L, Kang H, Wang T, Wen B, Wang Z, Jie J, Cao Z, Ruan H, Li T (2014) A promising new class of high-temperature alloys: eutectic high-entropy alloys. *Sci Rep* 4:6200
- [18] Li Z, Pradeep KG, Deng Y, Raabe D, Tasan CC (2016) Metastable high-entropy dual-phase alloys overcome the strength-ductility trade-off. *Nature* 534(7606):227
- [19] Jablonski PD, Licavoli JJ, Gao MC, Hawk JA (2015) Manufacturing of high entropy alloys. *JOM* 67(10):2278–2287
- [20] Guo S, Hu Q, Ng C, Liu CT (2013) More than entropy in high-entropy alloys: forming solid solutions or amorphous phase. *Intermetallics* 41:96–103
- [21] Ma L, Li C, Jiang Y, Zhou J, Wang L, Wang F, Cao T, Xue Y (2017) Cooling rate-dependent microstructure and mechanical properties of Al_xSi_{0.2}CrFeCoNiCu_{1-x} high entropy alloys. *J Alloys Compd* 694:61–67
- [22] Lv Y, Hu R, Yao Z, Chen J, Xu D, Liu Y, Fan X (2017) Cooling rate effect on microstructure and mechanical properties of Al_xCoCrFeNi high entropy alloys. *Mater Des* 132:392–399
- [23] King DJM, Middleburgh SC, McGregor AG, Cortie MB (2016) Predicting the formation and stability of single phase high-entropy alloys. *Acta Mater* 104:172–179
- [24] Ye YF, Wang Q, Lu J, Liu CT, Yang Y (2015) The generalized thermodynamic rule for phase selection in multi-component alloys. *Intermetallics* 59:75–80

- [25] Yang X, Zhang Y (2012) Prediction of high-entropy stabilized solid-solution in multi-component alloys. *Mater Chem Phys* 132:233–238
- [26] Tian F, Varga LK, Chen N, Delczeg L, Vitos L (2013) Ab initio investigation of high-entropy alloys of 3d elements. *Phys Rev B* 87(7):075144
- [27] Hsieh KC, Yu CF, Hsieh WT, Chiang WR, Ku JS, Lai JH, Tu CP, Yang CC (2009) The microstructure and phase equilibrium of new high performance high-entropy alloys. *J Alloys Compd* 483:209–212
- [28] Vida Á, Varga LK, Chinh NQ, Molnar D, Huang S, Vitos L (2016) Effects of the sp element additions on the microstructure and mechanical properties of NiCoFeCr based high entropy alloys. *Mater Sci Eng A* 669:14–19
- [29] Vida Á, Maksa Z, Molnár D, Huang S, Kovac J, Varga LK, Vitos L, Chinh NQ (2018) Evolution of the phase structure after different heat treatments in NiCoFeCrGa high entropy alloy. *J Alloys Compd* 743:234–239
- [30] Vida Á, Chinh NQ, Lendvai J, Heczal A, Varga LK (2017) Microstructures and transition from brittle to ductile behavior of NiFeCrMoW high entropy alloys. *Mater Lett* 195:14–17
- [31] Huang S, Vida Á, Li W, Molnár D, Kwon SK, Holmström E, Varga B, Varga LK, Vitos L (2017) Thermal expansion in FeCrCoNiGa high-entropy alloy from theory and experiment. *Appl Phys Lett* 110(24):241902
- [32] Pryds NH, Huang X (2000) The effect of cooling rate on the microstructures formed during solidification of ferritic steel. *Metall Mater Trans A* 31:3155–3166
- [33] Oliver W, Pharr G (1992) An improved technique for determining hardness and elastic modulus using load and displacement-sensing indentation systems. *J Mater Res* 7:1564–1583
- [34] Jones NG, Christofidou KA, Stone HJ (2015) Rapid precipitation in an Al_{0.5}CrFeCoNiCu high entropy alloy. *Mater Sci Technol* 31:1171–1177
- [35] Takeuchi A, Inoue A (2005) Classification of bulk metallic glasses by atomic size difference, heat of mixing and period of constituent elements and its application to characterization of the main alloying element. *Mater Trans* 46:2817–2829